AIAA JOURNAL
Vol. 41, No. 7, July 2003

Improved Turbulent Boundary-Layer Model for Shock Tubes

Eric L. Petersen*
University of Central Florida, Orlando, Florida 32816-2450
and
Ronald K. Hanson†
Stanford University, Stanford, California 94305

A viscous boundary-layer model was assembled to help describe the nonideal gas dynamics within shock tubes operating at high densities. The analytical model is based primarily on the landmark work of Mirels, who used the Blasius relation for the turbulent skin friction. The main improvement was the incorporation of a modern friction model for compressible, turbulent boundary layers via changes to the constants and exponents of Mirels's original boundary-layer relations. For example, the wall shear stress now depends on a Reynolds number to the −0.14 power as compared to −0.25 in the original model. As a result, the boundary layer at higher densities is thicker in the present model than in the original one, thus increasing the incident-shock attenuation and related nonuniformities. Even in borderline cases, the boundary-layer transitions to turbulent very quickly, usually within 100 μs for incident-shock pressures greater than about 2 atm. Because a turbulent boundary layer is thicker than a laminar one at the same conditions, the boundary-layer thickness in higher-pressure shock tubes is expected to be a larger fraction of the tube diameter than normally seen in lower-pressure shock tubes. The turbulent boundary layer and elevated pressure also increase the heat transfer to the shock-tube walls.

Nomenclature

A = constant in Van Driest II equation (32)
A' = constant in laminar boundary-layer heat transfer [Eq. (A9)]
a = sound speed of a perfect gas, $(\gamma RT)^{1/2}$
B = constant in Van Driest II equation (33)
B' = constant in turbulent boundary-layer heat transfer [Eq. (38)]
b = constant [Eq. (6)]
C_f = turbulent, compressible skin-friction coefficient
$C_{f,\delta}$ = C_f based on boundary-layer thickness
$C_{f,\theta}$ = C_f based on momentum thickness
$\bar{C}_f$ = turbulent, incompressible skin-friction coefficient
c = constant [Eq. (7)]
c_p = constant-pressure specific heat
$c_{p,e}$ = c_p at the edge of the boundary layer
$c_{p,m}$ = average c_p in the boundary layer
c_v = constant-volume specific heat
c_w = specific heat of shock-tube wall
c_1 = $[\beta(1+\alpha)]^{1/(1+\alpha)}$
c_2 = $c_1/(1+\alpha)$
D = shock-tube diameter
d = shock-tube hydraulic diameter, $4 \times \text{Area}/D$
F = T_w/T_e
F_{aw} = T_w/T_{aw}
F_c = boundary-layer skin-friction factor, $(\bar{C}_f/C_f)$
$F_{c,\text{SC}}$ = Spalding–Chi skin-friction factor
$F_{c,\text{VD}}$ = Van Driest II skin-friction factor
F_θ = boundary-layer Reynolds factor, $(\overline{Re}_\theta/Re_\theta)$
$F_{\theta,\text{SC}}$ = Spalding–Chi Reynolds factor
$F_{\theta,\text{VD}}$ = Van Driest II Reynolds factor
$f(\eta)$ = variable in Blasius boundary-layer momentum equation
I_N = integral solutions in boundary-layer equations [Eq. (10)]
k_e = bulk (initial) wall thermal conductivity
k_{o-} = wall thermal conductivity at surface
M = Mach number, u/a
$\bar{M}$ = molecular weight
M_e = freestream Mach number in shock-fixed frame
M_s = Mach number of incident shock wave (u_s/a_1)
m = compressible boundary-layer parameter, $0.5(\gamma-1)M_e^2$
n = $\alpha/(1+\alpha)$
P = static pressure
R = ideal gas constant, $R_u/\bar{M}$
R_u = universal gas constant, 8.314 kJ/kmol-K
Re = Reynolds number
Re_T = Reynolds number for transition to turbulence (6×10^5)
Re_δ = Reynolds number based on boundary-layer thickness $(u\delta/\nu)$
Re_θ = Reynolds number based on momentum thickness $(u\theta/\nu)$
$\overline{Re}_\theta$ = incompressible Re_θ
r = boundary-layer recovery factor $(\approx \sigma_m^{1/3} \approx 0.9)$
$r(\eta)$ = variable used in solution of Blasius boundary-layer equation
$s(\eta)$ = variable used in solution of Blasius boundary-layer equation
T = static temperature
T_{aw} = adiabatic wall temperature (i.e., T_r)
T_b = bulk temperature of shock tube (i.e., T_1)
T_e = freestream temperature in shock-fixed coordinates (T_2)
T_m = mean boundary-layer temperature, $0.5(T_w+T_\infty)+0.22(T_r-T_\infty)$
T_r = recovery temperature (i.e., T_{aw}); $T_e(1+ru_\infty^2/2c_{\text{p,m}})$
T_w = wall surface temperature
T_1 = initial gas temperature in driven section
T_2 = static temperature behind incident shock
t = time
u = axial velocity (i.e., one-dimensional velocity)
u_e = freestream velocity behind incident shock, shock-fixed coordinates $(|u_s|-u_2)$
u_s = incident-shock velocity in lab frame

Presented as Paper 2001-2855 at the AIAA 31st Fluid Dynamics Conference, Anaheim, CA, 11–14 June 2001; received 3 December 2001; revision received 11 October 2002; accepted for publication 23 January 2003.

*Assistant Professor, Mechanical, Materials and Aerospace Engineering. Member AIAA.
†Professor and Chair, Department of Mechanical Engineering. Fellow AIAA.

u_w = boundary-layer velocity at wall (i.e., $|u_s|$ in shock frame)
u_2 = gas velocity behind incident shock in lab frame
u_∞ = general freestream velocity outside of boundary layer
v = vertical velocity component in y direction
x = axial position behind shock in shock-fixed coordinates ($x = \bar{x} + u_w t$)
$\bar{x}$ = axial position in laboratory coordinates
α = exponent in turbulent friction factor [Eq. (17)]
α = thermal diffusivity ($k/\rho c_p$)
α_e = bulk wall thermal diffusivity
α_{o-} = wall thermal diffusivity at surface
α' = constant in Van Driest II relation [Eq. (30)]
β = constant in skin-friction factor
β' = constant in Van Driest II relation [Eq. (31)]
γ = specific heat ratio (c_p/c_v)
ΔT_w = wall temperature change, $T_w - T_b$
δ = boundary-layer thickness
δ^* = boundary-layer displacement thickness
η = boundary-layer similarity variable [Eq. (A2)]
θ = boundary-layer momentum thickness
μ = dynamic viscosity
μ_e = dynamic viscosity of freestream gas in shock-fixed coordinates
μ_m = mean boundary-layer viscosity
ν = kinematic viscosity (μ/ρ)
ν_e = kinematic viscosity of freestream gas in shock-fixed coordinates
ν_∞ = general kinematic viscosity of freestream gas
ξ = y/δ
ρ = static density of perfect gas (P/RT)
ρ_w = shock-tube wall material density
ρ_∞ = general freestream density
σ = Prandtl number ($c_p\mu/k$)
σ_e = Prandtl number of freestream gas in shock-fixed coordinates
σ_m = mean boundary-layer Prandtl number
τ_w = wall shear stress, $C_f \rho_e u_e^2/2$
ϕ = compressible boundary-layer scaling factor [Eq. (14)]
ψ = boundary-layer similarity variable

Subscripts

e = freestream condition
1 = initial condition in driven portion of shock tube (test section)
2 = condition behind the incident shock wave
4 = initial condition of the driver gas in the shock tube
5 = test-gas condition behind the reflected shock wave

Introduction

BECAUSE of wall viscous effects, a boundary layer forms behind the incident shock wave traveling down the driven section of a shock tube, as shown in Fig. 1. In the laboratory reference frame (Fig. 1a) the fluid in region 2 has zero velocity at the wall because of the no-slip boundary condition. However, in the shock reference frame (Fig. 1b) the wall moves with velocity $u_w = |u_s|$. The velocity profiles in both reference frames are defined in Fig. 1. Many theoretical treatments on shock-tube boundary layers have been performed over the last 40 years[1–9]; a review of work prior to 1964 is given by Spence and Woods.[10]

Of these shock-tube boundary-layer treatments, the approach adopted by most investigators is the one developed by Mirels and coworkers.[2–7] Numerous studies using low-pressure shock tubes have verified Mirels's general approach for both laminar and turbulent boundary layers,[11–14] although some authors believe the turbulent submodel to be inadequate.[15] The turbulent friction model in Mirels's original shock-tube boundary-layer formulas is, in fact, the focus of the present study. However, as discussed next, the compressible, turbulent friction model was based on one of the few in existence at the time of Mirels's original derivation.[3] Since then, data have become available that have led to better compressible skin-friction models that extend over wider Reynolds-number regions.

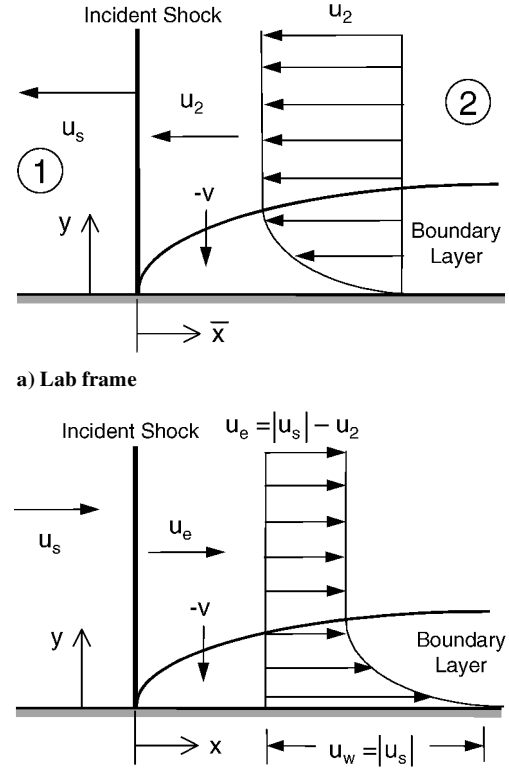

Fig. 1 Incident-shock coordinate systems showing boundary-layer velocity profiles.

This study was motivated by the impact of the incident-shock boundary layer (Fig. 1) on the test conditions at elevated pressures. In addition to affecting the conditions behind the incident shock wave, the boundary layer affects the conditions behind the reflected shock wave because the reflected wave propagates into a spatially and temporally varying flowfield containing a growing boundary layer.[16,17] At higher pressures and, hence, higher ρ and Reynolds numbers, the likelihood of a turbulent boundary layer increases. The turbulent boundary-layer model at elevated pressure, therefore, becomes particularly important.

A new turbulent boundary-layer model was added to the original formulation, the details of which are provided in this paper. Except where noted, the boundary-layer model is based exclusively on the original theory developed primarily by Mirels.[2–7] Presented next is a summary of the shock-tube boundary-layer equations and the original derivations of Mirels using the Blasius friction model. Details of the improved friction model and the modified boundary-layer relations are presented next, followed by sample calculations and comparisons with the original formulation. Further analysis can be found in Ref. 18, and experimental results of nonideal effects caused by the boundary layer in a high-pressure shock tube are provided in Ref. 19.

Turbulent Boundary-Layer Model

As for traditional flat-plate boundary-layer flow, the Reynolds number based on the freestream flow and axial position defines whether the boundary layer is laminar or turbulent. The accepted definition of the shock-tube Reynolds number, based on the laboratory reference frame, is[3,15]

$$Re = \rho_2 u_2^2 t / \mu_2 \tag{1}$$

where t is the time after arrival of the incident shock wave. Various experimenters have attempted to measure the transition Reynolds number Re_T with mixed results.[20–26] For the present work $Re_T \approx 6 \times 10^5$ (from Chabai and Emrich[20]) was selected because it

represented an average result from the limited range of available data.

For similar velocities and temperatures the density term in Eq. (1) increases linearly with the test pressure. Hence, an experiment that provides 50 atm behind the reflected shock wave (i.e., $P_2 \approx 12$ atm) has a Reynolds number that is 50 times greater than that of a typical shock-tube experiment with $P_5 = 1$ atm (i.e., $P_2 \approx 0.25$ atm). The likelihood of the boundary layer transitioning to turbulent rather quickly is therefore much greater in higher pressure experiments.

Throughout the present work conditions behind the incident shock wave (i.e., region 2) are based on the desired test conditions behind the reflected shock wave (i.e., region 5). This convention was chosen because most chemistry and shock-tunnel experiments are performed with the gas conditions behind the reflected shock wave. In other words, the present study assumes the incident-shock conditions are those that correspond to the stated reflected-shock conditions; from standard one-dimensional gas dynamics both states are functions only of M_s, γ, and the initial conditions (i.e., T_1 and P_1).

Provided in this section is a summary of the original turbulent boundary-layer relations for shock tubes, followed by their solution. A generic formulation of the results is then presented for convenient inclusion of the updated friction model.

Boundary-Layer Equations

The derivation of the compressible, turbulent boundary-layer equations used by Mirels[3] follows the traditional format, where the integral forms of the continuity and momentum equations are

$$\frac{\mathrm{d}}{\mathrm{d}x}\int_0^\infty \left(1 - \frac{\rho u}{\rho_e u_e}\right)\mathrm{d}y = \frac{\mathrm{d}\delta^*}{\mathrm{d}x} \tag{2}$$

$$\frac{\tau_w}{\rho_e u_e^2} = \frac{\mathrm{d}}{\mathrm{d}x}\int_0^\infty \frac{\rho u}{\rho_e u_e}\left(1 - \frac{u}{u_e}\right)\mathrm{d}y = \frac{\mathrm{d}\theta}{\mathrm{d}x} \tag{3}$$

Using the nondimensional variable $\xi = y/\delta$ and assuming, for analytical simplicity, a $\frac{1}{7}$-power law for the velocity profile relative to the moving wall (in shock-fixed coordinates; see Fig. 1):

$$\left|\frac{u - u_w}{u_e - u_w}\right| = \left(\frac{y}{\delta}\right)^{\frac{1}{7}} = \xi^{\frac{1}{7}} \qquad \text{for} \qquad 0 \le \xi \le 1 \tag{4a}$$

$$\left|\frac{u - u_w}{u_e - u_w}\right| = 1 \qquad \text{for} \qquad \xi > 1 \tag{4b}$$

Similarly, the density/temperature profile in the boundary layer can be shown to be

$$\rho_e/\rho = T/T_e = (T_w/T_e)\left(1 + b\xi^{\frac{1}{7}} - c\xi^{\frac{2}{7}}\right) \quad \text{for} \quad 0 \le \xi \le 1 \tag{5a}$$

$$\rho_e/\rho = T/T_e = 1 \quad \text{for} \quad 1 \le \xi \tag{5b}$$

where

$$b = T_r/T_w - 1 \tag{6}$$

$$c = (T_r/T_e - 1)(T_e/T_w) \tag{7}$$

Upon integrating Eqs. (2) and (3), the momentum and displacement thickness relations are obtained:

$$\delta^*/\delta = 1 - 7(T_e/T_w)[(u_w/u_e)I_6 + (1 - u_w/u_e)I_7] \tag{8}$$

$$\theta/\delta = 7(T_e/T_w)(1 - u_w/u_e)\{(u_w/u_e)I_6 + [1 - 2(u_w/u_e)]I_7 - (1 - u_w/u_e)I_8\} \tag{9}$$

The I_N in Eqs. (8) and (9) are defined by the integral

$$I_N = \int_0^1 \frac{z^N\,\mathrm{d}z}{1 + bz - cz^2} \tag{10}$$

The complete solution to Eq. (10) is quite lengthy and is given in detail in Appendix D of Mirels.[3]

At this stage the authors wish to point out the fact that the preceding boundary-layer relations and in the remainder of the paper are based on a two-dimensional boundary-layer approximation instead of an axisymmetric one. This approximation is often used for thin boundary layers in circular tubes. However, for relatively thick boundary layers in circular tubes the present model might underestimate the actual viscous effects.

Original Solution

If a constant wall temperature were assumed, θ/δ is independent of x, and Eq. (3) can be rewritten as

$$\frac{\tau_w}{\rho_e u_e^2} = \frac{\theta}{\delta}\frac{\mathrm{d}\delta}{\mathrm{d}x} \tag{11}$$

An expression for the wall friction is needed to integrate Eq. (11); in Mirels's work the Blasius relation for turbulent, incompressible flow over a flat plate was used:

$$\tau_w \Big/ \rho_\infty u_\infty^2 = \tfrac{1}{2}\bar{C}_f = 0.0225(\nu_\infty/u_\infty\delta)^{\frac{1}{4}} = 0.013(\nu_\infty/u_\infty\theta)^{\frac{1}{4}} \tag{12}$$

However, because Eq. (12) is for incompressible flow it was extended to compressible flow over a flat plate by using a suitable mean temperature T_m to define the average fluid properties. The resulting relations are

$$\tau_w \Big/ \rho_\infty u_\infty^2 = \tfrac{1}{2}C_f = 0.0225\phi_\infty(\nu_\infty/u_\infty\delta)^{\frac{1}{4}} \tag{13}$$

$$\phi_\infty = (\mu_m/\mu_\infty)^{\frac{1}{4}}(T_\infty/T_m)^{\frac{3}{4}} \tag{14}$$

$$T_m = 0.5(T_w + T_\infty) + 0.22(T_r - T_\infty) \tag{15}$$

When the wall is moving, as in the shock-fixed reference frame, one should use the velocities relative to the wall to be completely analogous to the Blasius formulation,[3] or

$$\tau_w \Big/ \rho_e u_e^2 = \tfrac{1}{2}C_f\left[(u_e - u_w)^2 \Big/ u_e^2\right] = 0.0225\phi(1 - u_w/u_e)|1 - u_w/u_e|^{\frac{3}{4}}(\nu_e/u_e\delta)^{\frac{1}{4}} \tag{16}$$

Generalized Solution

At the time of Mirels's calculations (i.e., 1956), the Blasius extrapolation [Eqs. (13) and (14)] was one of the more popular compressible-flow skin-friction correlations available. However, in the past 45 years a number of other compressible, flat-plate skin-friction relations have been developed. Additionally, the modern relations are more applicable to the larger Reynolds numbers of interest to high-pressure shock-tube flowfields. Therefore, the remaining equations for the turbulent boundary layer were rederived using a generic version of the wall friction relation, as follows:

$$\tau_w \Big/ \rho_\infty u_\infty^2 = \tfrac{1}{2}C_f = \beta\phi_\infty(\nu_\infty/u_\infty\delta)^\alpha = 0.578\beta\phi_\infty(\nu_\infty/u_\infty\theta)^\alpha \tag{17a}$$

$$\tau_w \Big/ \rho_e u_e^2 = \beta\phi(1 - u_w/u_e)|1 - u_w/u_e|^{1-\alpha}(\nu_e/u_e\delta)^\alpha \tag{17b}$$

$$\phi_\infty = (\mu_m/\mu_\infty)^\alpha(T_\infty/T_m)^{1-\alpha} \tag{18a}$$

$$\phi = (\mu_m/\mu_e)^\alpha(T_e/T_m)^{1-\alpha} \tag{18b}$$

The same form of the friction relation is used, but the constant and exponent are replaced by β and α, respectively, to keep the same format for the remaining attenuation and gas dynamic relations originally used by Mirels. Upon substituting Eq. (17b) into Eq. (11) etc., and integrating, the resulting relations for the boundary-layer

thickness, wall friction, and vertical displacement velocity are, respectively,

$$\delta = c_1 \left(\phi \frac{1 - u_w/u_e}{\theta/\delta} \right)^{1-n} \left(\frac{\nu_e}{u_e x} \right)^n \left| 1 - \frac{u_w}{u_e} \right|^{(1-\alpha)/(1+\alpha)} \tag{19}$$

$$\frac{\tau_w}{\rho_e u_e^2} = c_2 \frac{\theta}{\delta} \left(\phi \frac{1 - u_w/u_e}{\theta/\delta} \right)^{1-n} \left(\frac{\nu_e}{u_e x} \right)^n \left| 1 - \frac{u_w}{u_e} \right|^{(1-\alpha)/(1+\alpha)} \tag{20}$$

$$\frac{v_e}{u_e} = \frac{\mathrm{d}\delta^*}{\mathrm{d}x} = c_2 \frac{\delta^*}{\delta} \left(\phi \frac{1 - u_w/u_e}{\theta/\delta} \right)^{1-n} \left(\frac{\nu_e}{u_e x} \right)^n \left| 1 - \frac{u_w}{u_e} \right|^{(1-\alpha)/(1+\alpha)} \tag{21}$$

where

$$n = \alpha/(1+\alpha) \tag{22}$$

$$c_1 = [\beta(1+\alpha)]^{1/(1+\alpha)} \tag{23}$$

$$c_2 = c_1/(1+\alpha) \tag{24}$$

If the Blasius expression for skin friction were employed [Eq. (16)], the value for n would be $\frac{1}{5}$, as in Mirels.[3]

Improved Friction Model

Over the past several decades, a number of empirical skin-friction relations have been developed for turbulent, compressible flowfields.[27–32] The turbulent, compressible skin-friction coefficient C_f is generally based on the incompressible skin-friction coefficient, for which many measurements are available:

$$\bar{C}_f = F_c C_f \tag{25}$$

Hopkins and Inouye[28] suggested the use of the Kármán–Schoenherr relation for the incompressible skin friction:

$$1/\bar{C}_f = 17.08(\log_{10} \overline{Re}_\theta)^2 + 25.11 \log_{10} \overline{Re}_\theta + 6.012 \tag{26}$$

which was adopted for the calculations herein. The incompressible Reynolds number is related to the compressible Reynolds number as follows:

$$\overline{Re}_\theta = F_\theta Re_\theta \tag{27}$$

Various relations are available for the factors F_c and F_θ, the relative benefits and applicability of which have been compared by previous investigators.[27–32] Among the relations are those attributed to White and Christoph, Van Driest, Spalding–Chi, Coles, and Eckert. Of these methods, the Van Driest II and Spalding–Chi models are preferred in the literature.[28,29] These two expressions were considered in the present study and are summarized as follows.

Van Driest II:

$$F_{c,\mathrm{VD}} = \frac{rm}{(\sin^{-1}\alpha' + \sin^{-1}\beta')^2} \tag{28}$$

$$F_{\theta,\mathrm{VD}} = \frac{\mu_e}{\mu_w} \tag{29}$$

$$\alpha' = \frac{(2A^2 - B)}{\sqrt{4A^2 + B^2}} \tag{30}$$

$$\beta' = \frac{B}{\sqrt{4A^2 + B^2}} \tag{31}$$

$$A = \sqrt{rm/F} \tag{32}$$

$$B = \frac{(1 + rm - F)}{F} \tag{33}$$

Spalding and Chi:

$$F_{c,\mathrm{SC}} = \text{same as Van Driest II [Eq. (28)]}$$

$$F_{\theta,\mathrm{SC}} = 1 \Big/ F^{0.702} F_{\mathrm{aw}}^{0.772} \tag{34}$$

In the preceding equations $F = T_w/T_e$, and $F_{\mathrm{aw}} = T_w/T_{\mathrm{aw}}$.

One goal of the current work was to put either the Van Driest II or Spalding–Chi (or both) relations for the skin friction into the form of Eq. (17a). Of course, Eq. (17a) is based on Re_δ, whereas the newer friction relations [Eqs. (28–34)] are based on Re_θ. For simplicity, the conversion factor was taken from the ratio used by Blasius [Eq. (12)] because $\theta/\delta = 7/72$ (Refs. 28 and 33). Although this ratio actually varies with the level of compressibility in the flow, the authors feel that the resulting relation between Re_δ and Re_θ is within the accuracy of the overall model described herein.

The procedure for putting the turbulent, compressible friction models into the form of Eq. (17a) was as follows. A parametric data set of realistic shock-tube conditions in argon was compiled, corresponding to conditions of $P_5 = 1$, 50, 100, 200, 500, and 1000 atm; $M_s = 2.0, 2.4, 2.8$, and 3.2 (i.e., $T_5 = 1035, 1438, 1912$, and 2457 K); and θ covering the range of 0.1–25 mm. The analogous Re_θ and ϕ ranged from approximately 100 to 10^8 and 1.14 to 1.24, respectively. For each parametric combination of conditions, the Spalding–Chi, Van Driest II, and Blasius friction models were computed. Figure 2 compares the results for each model, where the newer correlations predict C_f that are nearly a factor of two larger than the Blasius C_f for higher Re_θ (i.e., $>10^4$). At lower Re_θ the newer correlations, particularly the Van Driest II model, predict C_f that coincide with those of the Blasius model.

Also shown in Fig. 2 are the curve fits to the Van Driest II and Spalding–Chi relations in the form of Eq. (17a). For the Spalding–Chi model the curve fit gives $\beta = 0.0077$ and $\alpha = 0.14$; the curve fit for the Van Driest II calculations gives $\beta = 0.0103$ and $\alpha = 0.15$. Although either friction model can be employed, the Spalding–Chi version was selected herein because it provided a slightly better visible fit to the desired form for $Re_\theta > 10^4$. Therefore, at higher Reynolds number and densities the following friction relation was employed[18]:

$$\tau_w \Big/ \rho_e u_e^2 = 0.0077 \phi (1 - u_w/u_e) |1 - u_w/u_e|^{0.86} (\nu_e/u_e \delta)^{0.14} \tag{35}$$

However, at lower densities the Blasius expression originally used by Mirels can still be utilized. As will be discussed further in the following, the cutoff test pressure (P_5) between high and low densities is around 1 atm. (Note that, at the lower densities, the boundary layer can remain laminar for some time, so that the particular turbulent friction model employed is not as critical.)

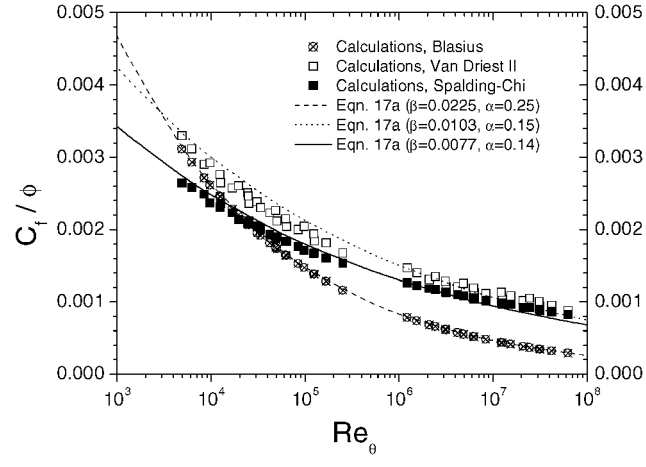

Fig. 2 Comparison between modern (Spalding–Chi and Van Driest II) and original Blasius wall skin-friction coefficient for compressible, turbulent flow. The Spalding–Chi model was chosen for the calculations herein.

Wall Heat Transfer

Because convective heat transfer to the shock-tube walls increases with pressure, wall heating is expected to be higher at elevated pressures than in conventional, low-pressure shock tubes for combustion chemistry measurements. The heat-transfer equations defining the T_w increase behind the incident shock wave are summarized in this section. The relations used herein were modified from those derived by Mirels[3]; similar relations have been derived by others.[34] Turbulent boundary-layer heat transfer is covered in this section; laminar boundary-layer heat transfer is considered in the Appendix. As was done for the boundary-layer relations, the exponents in the heat-transfer relation were put into a general form for easy incorporation of the improved friction model.

An important reference temperature in compressible boundary layers and heat transfer is the adiabatic-wall, or reduced, temperature. It is estimated as[3]

$$\frac{T_r}{T_e} = 1 + \left(\frac{u_w}{u_e} - 1\right)^2 \frac{r u_e^2}{2 T_e c_{\mathrm{p,m}}} \tag{36}$$

Using the Reynolds analogy between wall viscous and heat-transfer effects, the increase in wall surface temperature for a turbulent boundary layer behind the incident shock wave follows the relation

$$\frac{T_w - T_b}{T_b} = B' \frac{[(T_r/T_b) - 1]}{1 + B'} \tag{37}$$

where

$$B' = c_2 \sqrt{\pi} \phi^{1-n} \frac{c_{\mathrm{p,m}}}{c_{\mathrm{p,e}}} \left(\frac{\sigma_m}{\sigma_e}\right)^{-\frac{2}{3}} \sigma_e^{-\frac{1}{6}} \left(\frac{\theta/\delta}{1 - u_w/u_e}\right)^n \times \left|1 - \frac{u_w}{u_e}\right|^{(1-\alpha)/(1+\alpha)} \sqrt{\frac{u_e}{u_w}} \sqrt{\frac{\alpha_{o-}}{\alpha_e}} \frac{k_e}{k_{o-}} \left(\frac{x u_e}{\nu_e}\right)^{\sqrt{(1-\alpha)/(1+\alpha)}} \tag{38}$$

Therefore,

$$\Delta T_w \propto \rho_e^{\sqrt{(1-\alpha)/(1+\alpha)}} (k_e \rho_e c_p)^{\frac{1}{2}}$$

From Eq. (35) for the skin friction (i.e., $\alpha = 0.14$), the pressure dependence of the wall temperature increase is $P^{1.37}$. The turbulent wall heat transfer is hence more pressure sensitive ($P^{1.37}$) than the laminar wall heat transfer ($P^{0.5}$; see Appendix).

Results

This section presents the results of calculations using the model just described over a wide range of test temperatures and pressures for an argon test gas and a helium driver gas. The boundary-layer relations and the usual one-dimensional shock-tube relations were programmed into a computer program written and compiled using Digital Visual FORTRAN. Boundary-layer thickness δ is defined herein as the edge of the layer where the velocity is 99% of u_e. Results for δ are covered first, followed by calculations of the wall temperature increase.

In general, the results were calculated at a fixed axial location after passage of the incident shock wave in the laboratory reference frame. This situation is analogous to the boundary layer starting at time zero with zero thickness immediately upon passage of the shock; the layer then grows with time at the fixed location. Conversely, one can think of the situation relative to the shock wave, where the boundary layer starts immediately behind it and increases in thickness with distance behind the shock. The difference between the two reference frames is simply a conversion between distance behind the shock x and time t, which are related via $x = \bar{x} + u_w t$.

Reflected-shock arrival is not included in the calculations because the present treatment of the boundary-layer growth is not valid behind the reflected shock. Nonetheless, most of the results are presented in terms of the conditions behind the reflected shock wave (i.e., T_5 and P_5) because these are the parameters of concern for the experiments of primary interest.[18] The corresponding conditions behind the incident shock (i.e., T_2 and P_2) and the shock speed are provided when appropriate.

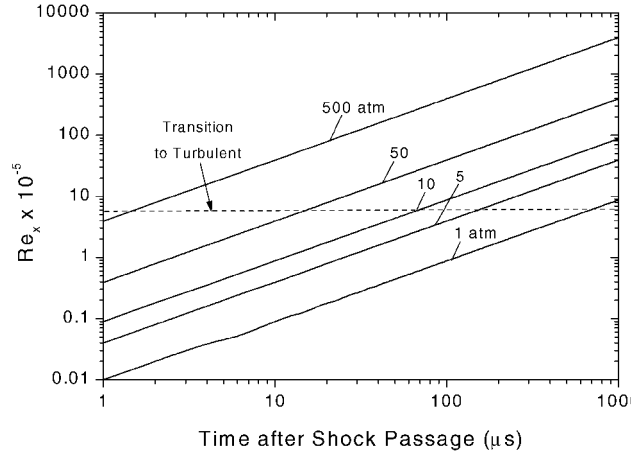

Fig. 3 Flow Reynolds number [Eq. (1)] after incident-shock passage in argon for various pressures. $T_5 = 1800$ K; listed pressures are P_5 conditions. Turbulence occurs when $Re_x = Re_T \approx 6 \times 10^5$.

Boundary-Layer Thickness

Immediately behind the incident shock wave, the boundary layer starts out laminar but eventually transitions to turbulent. The time/distance at which this transition occurs depends on Re_x and, hence, the test conditions. Using the already defined Re_T of 6×10^5, the time at which the transition takes place can be estimated. Figure 3 shows the results of such a calculation over a range of test pressures for an 1800-K test temperature ($M_s = 2.74$). For conditions leading to a test pressure of 1 atm, the boundary layer can remain laminar for some time, almost 1 ms after shock passage. However, at elevated pressures the boundary layer transitions to turbulent rather quickly, within 10 μs for P_5 greater than about 50 atm ($P_2 > 13$ atm). One can safely conclude from Fig. 3 that the boundary layer is entirely turbulent at higher pressures without introducing significant error.

The growth of the boundary layer as a function of time after shock passage is presented in Fig. 4 at three test pressures: 1, 50, and 500 atm. In each plot the results of the new model for a wholly turbulent boundary layer are compared to the results using Mirels' model for a completely turbulent layer and to the results assuming a fully laminar layer. At the lower pressure of 1 atm ($P_1 = 0.03$ atm) in Fig. 4a, the predictions of $\delta(t)$ for both the new model and the original model of Mirels are nearly identical.

However, noticeable deviations occur at higher pressures, where the boundary-layer growth predicted by the improved model is about 50% higher at 50 atm (Fig. 4b) and nearly 100% higher at 500 atm (Fig. 4c) than that of the original model. Additionally, in each plot in Fig. 4 the turbulent boundary layer is considerably thicker than the laminar boundary layer. The difference is at least a factor of 10 or more after 1 ms. Hence, significant error can result if one were to assume a laminar boundary layer when the Reynolds number is high enough for the layer to actually be turbulent.

Upon comparing the magnitude of δ in each Fig. 4 plot, the effect of pressure can be discerned. As expected, the boundary-layer thickness decreases with increasing pressure for a fully turbulent layer. Figure 5 summarizes the effect of test temperature (i.e., shock speed) on $\delta(t)$ as predicted by the improved model. At higher test temperatures the boundary layer is thicker.

Although the calculations thus far have assumed either a fully turbulent or a fully laminar boundary layer, it is useful to combine the two solutions for intermediate Reynolds number as is often done.[27,33] Using a Re_T of 6×10^5, the transition between laminar and turbulent can be approximated. Some sample results are provided in Fig. 6 for $M_s = 2.74$ ($T_5 = 1800$ K) for a range of P_5 from 1 to 500 atm. The transition and corresponding increase in growth

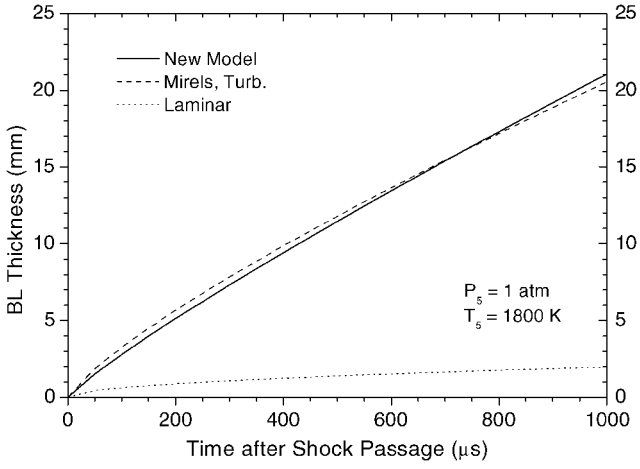

a) $P_5 = 1$ atm ($P_2 = 0.3$ atm)

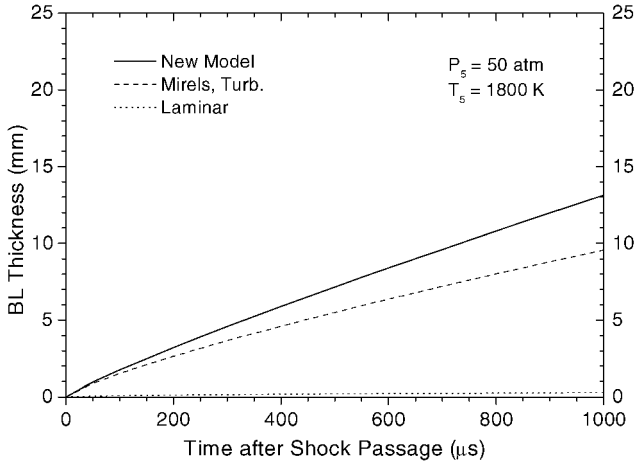

b) $P_5 = 50$ atm ($P_2 = 12.3$ atm)

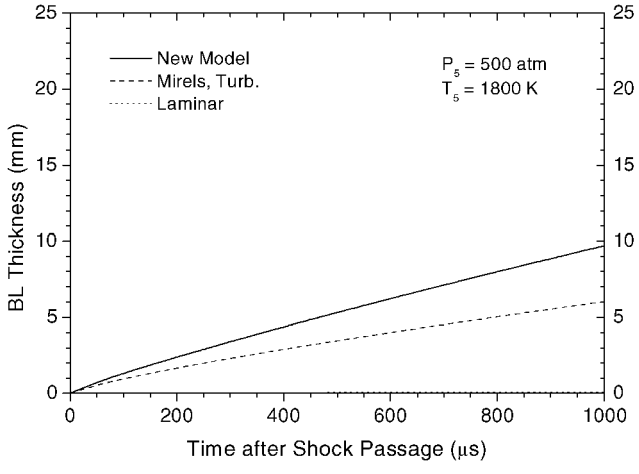

c) $P_5 = 500$ atm ($P_2 = 123$ atm)

Fig. 4 Predictions of boundary-layer thickness at a fixed location after passage of the incident shock wave. $T_5 = 1800$ K ($T_2 = 943$ K; $M_s = 2.74$); argon.

rate is clear at the lower pressures, whereas the higher pressures force the boundary layer to become turbulent almost instantly.

Another useful calculation involves estimating δ at a fixed location at the instant the reflected shock wave reaches that point. This is analogous to measurements being performed behind the reflected shock wave at a test port located a finite distance from the shock-tube end wall. Assuming a port located 2 cm from the end wall and a shock speed providing a test temperature of either 1400 or 2000 K, the boundary-layer thickness at the time of reflected shock arrival is as shown in Fig. 7 as a function of pressure. The results

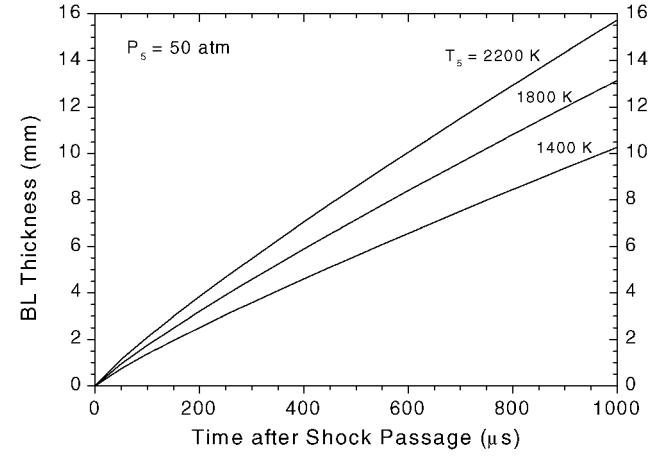

Fig. 5 Effect of test temperature on boundary-layer growth behind the incident shock wave at a fixed axial location. Conditions correspond to $P_5 = 50$ atm. The $T_5 = 2200$, 1800, and 1400 K correspond to $T_2 = 1110$ K ($M_s = 3.05$), 943 K (2.74), and 775 K (2.39).

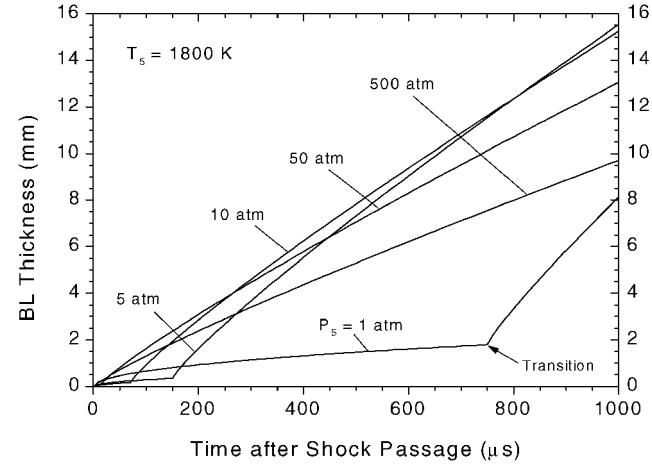

Fig. 6 Prediction of δ at a fixed axial location assuming a transition from laminar to turbulent using the new friction model. Conditions correspond to $T_5 = 1800$ K ($T_2 = 943$ K; $M_s = 2.74$) in argon.

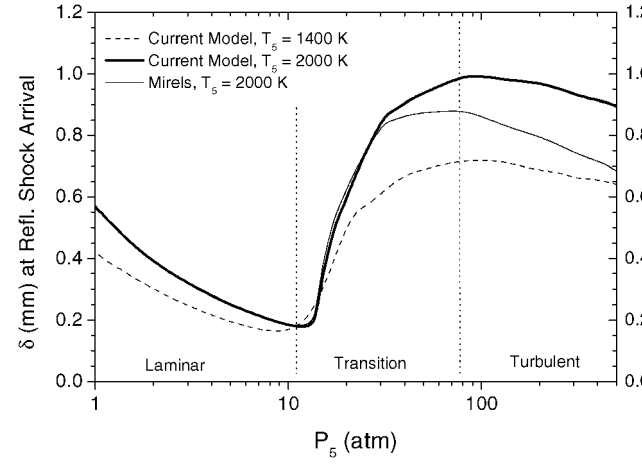

Fig. 7 Calculated boundary-layer thickness in argon at an axial position 20 mm upstream of the end wall at the time of reflected-shock arrival for various pressures and temperatures. The transition from laminar to turbulent is included. Also shown is the prediction using the original friction model.[3]

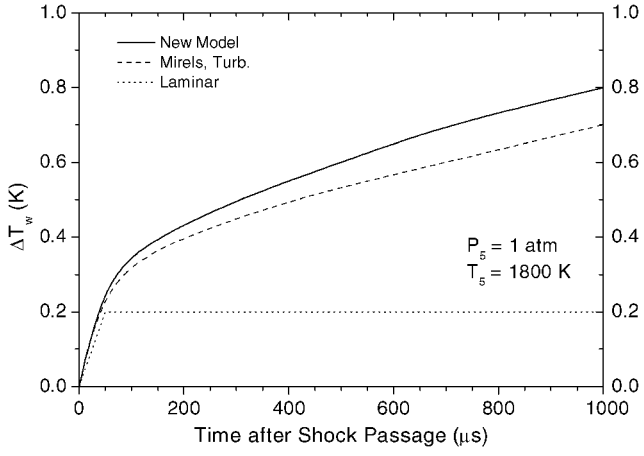

a) $P_5 = 1$ atm ($P_2 = 0.3$ atm)

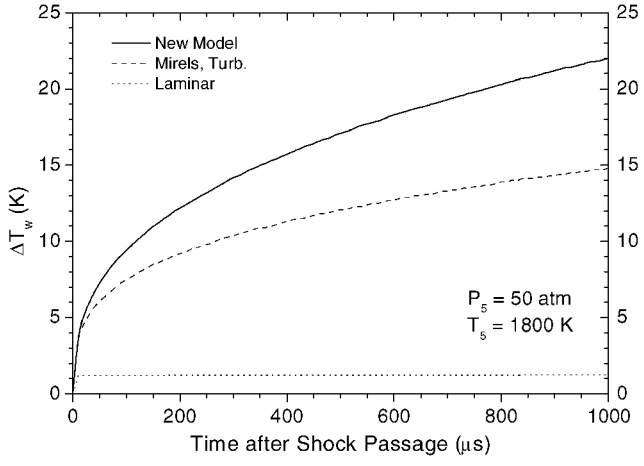

b) $P_5 = 50$ atm ($P_2 = 12.3$ atm)

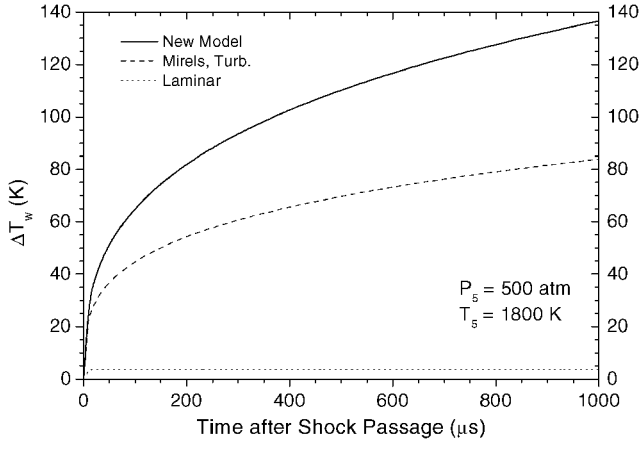

c) $P_5 = 500$ atm ($P_2 = 123$ atm)

Fig. 8 Side-wall temperature increase at a fixed axial location after passage of the incident shock wave for three different pressures. $T_5 = 1800$ K ($M_s = 2.74$); argon.

in Fig. 7 are from the combined laminar and turbulent solutions, as in Fig. 6. Also provided for comparison are the results of the original model. The regions of test pressure where the boundary layer is laminar, transitional, or turbulent at the time of reflected-shock arrival are evident. The improved model agrees with Mirels's results for $P_5 < 30$ atm but predicts larger δ for $P_5 > 30$ atm.

Wall Temperature

According to Eqs. (37) and (38), the side-wall surface temperature is expected to increase with increasing pressure per $P^{1.37}$ when the boundary layer is fully turbulent. This pressure dependence is

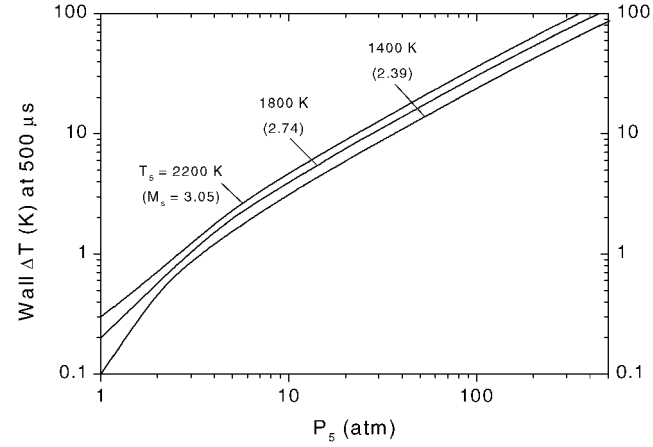

Fig. 9 Effect of test pressure and temperature on side-wall temperature increase, 500 μs after passage of the incident shock wave, using the improved model. The arrival of the reflected wave is not included.

greater than that of the Blasius friction model, where $\Delta T_w \propto P^{1.27}$. Figure 8 presents the estimated increase in wall temperature as a function of time after incident-shock passage for $M_s = 2.74$ and three test pressures: 1, 50, and 500 atm. At the lowest pressure (Fig. 8a) the wall temperature increase is negligible (<1 K) after 1 ms. However, the higher pressures (Figs. 8b and 8c) lead to temperature increases as great as 100 K or more. In all cases considered in Fig. 8, the ΔT_w is negligible if the assumption of a fully laminar boundary layer were used.

A summary of the wall temperature increase using the improved model only is provided in Fig. 9. The ΔT in Fig. 9 correspond to a time 500 μs after passage of the incident shock wave. The wall heat transfer increases with increasing test temperature and increasing test pressure.

Discussion

From the preceding results the improved shock-tube boundary-layer model predicts larger shock-tube nonidealities as a result of the boundary layer than does the original model when the Reynolds numbers are large enough for the layer to be completely turbulent. In addition, the model predicts that higher pressure shock tubes ($P_5 > 1$ atm), in general, should have greater losses as a result of viscous effects than typically expected from lower pressure shock tubes ($P_5 < 1$ atm). A thicker boundary layer also has more impact in smaller diameter shock tubes than larger diameter ones because the layer comprises a greater fraction of the total flow area.

Among the primary repercussions from these nonideal effects is the result that the test temperatures and pressures vary with time and, hence, differ from ideal shock-tube behavior. The properties behind the incident wave vary with time because the boundary layer bleeds fluid from the uniform core flow, creating disturbance waves that propagate downstream. These disturbance waves also interact with and attenuate the incident shock wave.[35–44] The temperature and pressure behind the reflected shock wave change with time because the reflected wave is traveling into the temporally and spatially nonuniform flowfield induced by the boundary layer.[15–19]

Additional details on the analytical treatment of nonideal gas dynamics caused by the turbulent boundary layer are provided in Petersen.[18] A complete model of the nonuniformities behind the incident shock wave, also based on the landmark work of Mirels and coworkers,[4,7,40,44] was developed by the authors.[18] A separate model for the conditions behind the reflected shock wave that builds on the incident-shock model is summarized and compared to experimental results of Petersen and Hanson.[19]

Finally, the heat transfer to the shock-tube walls is higher for the current model when compared to the original one (Fig. 8). The wall temperature increase is likewise greater at elevated pressures than at conditions giving reflected-shock pressures near 1 atm or less. Although a secondary effect, hotter shock-tube walls can have

an adverse impact on certain measurements. For example, increased heat transfer to side-wall pressure transducers can lead to anomalous results,[19,45] and hotter walls emit greater levels of background, interference radiation when conducting spectroscopic measurements using infrared emission.[46]

Conclusions

An improved turbulent boundary-layer model for shock tubes was presented. Based on the original shock-tube boundary-layer equations of Mirels, the primary improvement in the new model was in the compressible, turbulent friction term. Both the Van Driest II and Spalding–Chi friction models were incorporated into the shock-tube boundary-layer relations via curve fits to keep the same form as the original expression used by Mirels (i.e., the Blasius model). Therefore, only modifications to a few constants and exponents were needed to incorporate the updated friction results into the solution of the boundary-layer relations. Although the Spalding–Chi model was chosen for the calculations herein, either model can be employed per the user's preference.

Although the improved model can be used for turbulent boundary layers in all shock tubes, it is particularly useful for modeling higher pressure shock tubes where the larger Reynolds numbers lead to early boundary-layer transition to turbulence. Because the Spalding–Chi friction coefficient is larger than the Blasius coefficient at larger Reynolds numbers, the predicted boundary-layer thickness in the present model can be 50–100% greater than the thickness predicted by the original one for conditions leading to test pressures greater than about 10 atm. The net result is that nonidealities in the shock-tube gas dynamics caused by viscous effects are expected to be greater in high-pressure shock tubes, where the boundary layer is predominately turbulent, than in conventional-pressure tubes. Similarly, the higher pressure and turbulent boundary layer enhance the heat transfer to the shock-tube wall, increasing the postshock wall temperature by as much as 100 K at conditions corresponding to 500 atm behind the reflected wave (i.e., $P_2 = 130$ atm).

Appendix: Laminar Boundary Layer

The laminar boundary-layer model is based entirely on the theory developed by Mirels.[2] Although the calculations for high-pressure shock tubes should assume a fully turbulent boundary layer behind the incident shock wave, the laminar model is included for the lower pressure (i.e., lower Reynolds numbers) cases, as in Fig. 6. In addition, the laminar model (valid for $Re < 6 \times 10^5$) can be used in shock-tube calculations for conventional, low-pressure (<1 atm) facilities. Provided next is a summary of the model for completeness.

Laminar Boundary-Layer Model

In general, the laminar boundary-layer equations are based on the classical equations of Blasius and the fourth-order polynomial, Kármán–Pohlhausen solution. It is assumed that the gas thermal conductivity and viscosity scale linearly through the boundary layer with temperature [i.e., $k = k_w(T/T_w)$ and $\mu = \mu_w(T/T_w)$], and c_p and σ are constant and equal to $c_{p,w}$ and σ_w.

Using the boundary-layer model of Fig. 1, the Blasius differential equation for momentum is

$$f''' + ff'' = 0, \qquad f(0) = 0$$
$$f'(0) = u_w/u_e, \qquad f'(\infty) = 1 \tag{A1}$$

where η and ψ are the usual similarity variables modified for compressible flow[2]:

$$\eta = \sqrt{\frac{u_e}{2x\nu_w}} \int_0^y \frac{T_w}{T}\,\mathrm{d}y \tag{A2}$$

$$\psi = f(\eta)\sqrt{2u_e x \nu_w} \tag{A3}$$

The solution to the energy equation involves the dependent variables $r(\eta)$ and $s(\eta)$ as follows:

$$r''' + \sigma f r' = \frac{-2\sigma_w}{(u_w/u_e - 1)^2}(f'')^2, \qquad r(\infty) = r'(0) = 0 \tag{A4}$$

$$s'' + \sigma f s' = 0, \qquad s(0) = 1, \qquad s(\infty) = 0 \tag{A5}$$

The wall shear stress is then obtained as

$$\tau_w = \left(\mu \frac{\partial u}{\partial y}\right)_w = u_e f''(0)\sqrt{\frac{u_e \rho_w u_w}{2x}} \tag{A6}$$

In similar fashion the important boundary-layer parameters such as δ, θ, v_e, etc., are obtained.[2,3] The boundary layer T is a function of $r(\eta)$ and $s(\eta)$:

$$T/T_e = 1 + [(\gamma - 1)/2]\left[(u_w/u_e - 1)M_e^2\right]^2 r(\eta) + (T_w/T_e - T_r/T_e)s(\eta) \tag{A7}$$

To obtain T_r in Eq. (A7), $r(0)$—the recovery factor—is needed and is assumed to be $\approx$0.85. The solution techniques for Eqs. (A1–A5) are covered in detail in Mirels[2]; the primary modification/update to the way Mirels solved the equations was the use of modern numerical techniques such as the shooting method for solving Eq. (A1).

However, in a later effort Mirels derived simplified solutions to Eqs. (A1), (A4), and (A5) using a Kármán–Pohlhausen integral technique to obtain closed-form expressions for η, $r(0)$, $s'(0)$, $f''(0)$, etc. These results can be found in Ref. 3.

Wall Heat Transfer

For the laminar boundary layer the temperature increase at the wall surface is[2]

$$\frac{T_w - T_b}{T_b} = A' \frac{[(T_r/T_b) - 1]}{1 + A'} \tag{A8}$$

where

$$A' = \frac{-s'(0)}{\sqrt{(2/\pi)\sigma_e}} \sqrt{\frac{u_e}{u_w}} \sqrt{\frac{\alpha_{o-}}{\alpha_w}} \frac{k_w}{k_{o-}} \tag{A9}$$

and, for $u_w/u_e > 1$,

$$\frac{T_r}{T_b} - 1 = \left(\frac{u_w}{u_e} - 1\right)\left\{\frac{(u_w/u_e + 1) + (u_w/u_e - 1)r(0)}{(u_w/u_e)[(\gamma + 1)/(\gamma - 1) - u_w/u_e]}\right\} \tag{A10}$$

From Eq. (A8) and because A' is a small number, the increase in wall surface temperature relative to the initial, or bulk, temperature of the wall is proportional to $\sqrt{(k_e \rho_e c_{p,e})}$. Therefore, the wall temperature increase for a laminar boundary layer behind the incident shock wave is $\propto P^{0.5}$.

Acknowledgments

The initial derivations and calculations in this paper were performed at Stanford University with the support of the Office of Naval Research, with Richard Miller as the Program Monitor. Further analyses, calculations, and all of the writing were performed at The Aerospace Corporation for the Air Force Space and Missile Systems Center under Contract F04701-00-C-0009 and at the University of Central Florida.

References

[1] Trimpi, R. L., and Cohen, N. B., "A Theory for Predicting the Flow of Real Gases in Shock Tubes with Experimental Verification," NACA TN 3375, March 1955.

[2] Mirels, H., "Laminar Boundary Layer Behind Shock Advancing into Stationary Fluid," NACA TN 3401, March 1955.

[3] Mirels, H., "Boundary Layer Behind Shock or Thin Expansion Wave Moving into Stationary Fluid," NACA TN 3712, May 1956.

[4] Mirels, H., "Shock Tube Test Time Limitation due to Turbulent-Wall Boundary Layer," *AIAA Journal*, Vol. 2, No. 1, 1964, pp. 84–93.

[5]Mirels, H., and King, W. S., "Series Solution for Shock-Tube Laminar Boundary Layer and Test Time," *AIAA Journal*, Vol. 4, No. 5, 1966, pp. 782–789.

[6]Mirels, H., "Correlation Formulas for Laminar Shock Tube Boundary Layer," *Physics of Fluids*, Vol. 9, No. 7, 1966, pp. 1265–1272.

[7]Mirels, H., "Boundary Layer Growth Effects in Shock Tubes," *Shock Tube Research, Proceedings of the Eighth International Shock Tube Symposium*, edited by J. L. Stollery, A. G. Gaydon, and P. R. Owen, Chapman and Hall, London, 1972, pp. 6/2–30.

[8]Akamatsu, T., and Urushidani, H., "A Generalized Solution of Quasi-Steady Laminar Flat Plate Boundary Layer in a Shock Tube," *Bulletin of the Japan Society of Mechanical Engineers*, Vol. 12, No. 52, 1969, pp. 793–801.

[9]Doolan, C. J., and Jacobs, P. A., "Modeling Mass Entrainment in a Quasi-One-Dimensional Shock Tube Code," *AIAA Journal*, Vol. 34, No. 6, 1996, pp. 1291–1293.

[10]Spence, D. A., and Woods, B. A., "A Review of Theoretical Treatments of Shock-Tube Attenuation," *Journal of Fluid Mechanics*, Vol. 19, 1964, pp. 161–174.

[11]Emrich, R. J., and Wheeler, D. B., Jr., "Wall Effects in Shock Tube Flow," *Physics of Fluids*, Vol. 1, No. 1, 1958, pp. 14–23.

[12]Gion, E. J., "Measured Velocity Profiles in the Laminar Boundary Layer Behind a Shock," *Physics of Fluids*, Vol. 8, No. 3, 1965, pp. 546, 547.

[13]Fox, J. N., McLaren, T. I., and Hobson, R. M., "Test Time and Particle Paths in Low-Pressure Shock Tubes," *Physics of Fluids*, Vol. 9, No. 12, 1966, pp. 2345–2350.

[14]Hubbard, E. W., and de Boer, P. C. T., "Flow Field Behind a Shock Wave in a Low-Pressure Test Gas," *Physics of Fluids*, Vol. 12, No. 12, 1969, pp. 2515–2521.

[15]Fujii, N., Koshi, M., Ando, H., and Asaba, T., "Evaluation of Boundary-Layer Effects in Shock-Tube Studies of Chemical Kinetics," *International Journal of Chemical Kinetics*, Vol. 11, 1979, pp. 285–304.

[16]Rudinger, G., "Effect of Boundary Layer Growth in a Shock Tube on Shock Reflection from a Closed End," *Physics of Fluids*, Vol. 4, 1961, pp. 1463–1473.

[17]Hanson, R. K., "Shock Wave Reflexion in a Relaxing Gas," *Journal of Fluid Mechanics*, Vol. 45, 1971, pp. 721–746.

[18]Petersen, E. L., "A Shock Tube and Diagnostics for Chemistry Measurements at Elevated Pressures with Application to Methane Ignition," Ph.D. Dissertation, Dept. of Mechanical Engineering, Stanford Univ., Stanford, CA, March 1998.

[19]Petersen, E. L., and Hanson, R. K., "Nonideal Effects Behind Reflected Shock Waves in a High-Pressure Shock Tube," *Shock Waves*, Vol. 10, No. 6, 2001, pp. 405–420.

[20]Chabai, A. J., and Emrich, R. J., "Transition from Laminar to Turbulent Flow in the Shock Tube Boundary Layer," *Bulletin of the Americal Physical Society*, Ser. II, Vol. 3, 1958, p. 291.

[21]Mark, H., and Mirtich, M. J., Jr., "Transition in Shock-Tube Boundary Layers," *Physics of Fluids*, Vol. 5, No. 2, 1962, pp. 251–253.

[22]Thompson, W. P., and Emrich, R. J., "Turbulent Spots and Wall Roughness Effects in Shock Tube Boundary Layer Transition," *Physics of Fluids*, Vol. 10, No. 1, 1967, pp. 17–20.

[23]Boison, J. C., "Highly Cooled Boundary Layer Transition Data in a Shock Tube," *Modern Developments in Shock Tube Research*, *Proceedings of the Tenth International Shock Tube Symposium*, edited by G. Kamimoto, Shock Tube Research Society, Kyoto, Japan, 1975, pp. 127–140.

[24]Brun, R., Auberger, P., and Van Qué, N., "Shock Tube Study of Boundary Layer Instability," *Acta Astronautica*, Vol. 5, 1978, pp. 1145–1152.

[25]Chaney, M. J., and Cook, W. J., "Further Experiments on Shock Tube Wall Boundary-Layer Transition," *AIAA Journal*, Vol. 21, No. 7, 1983, pp. 1046–1048.

[26]Brun, R., "Comment on 'Further Experiments on Shock-Tube Wall Boundary-Layer Transition,'" *AIAA Journal*, Vol. 23, No. 8, 1985, pp. 1297–1299.

[27]White, F. M., *Viscous Fluid Flow*, 2nd ed., McGraw–Hill, New York, 1991.

[28]Hopkins, E. J., and Inouye, M., "An Evaluation of Theories for Predicting Turbulent Skin Friction and Heat Transfer on Flat Plates at Supersonic and Hypersonic Mach Numbers," *AIAA Journal*, Vol. 9, No. 6, 1971, pp. 993–1003.

[29]Cary, A. M., Jr., and Bertram, M. H., "Engineering Prediction of Turbulent Skin Friction and Heat Transfer in High-Speed Flow," NASA TN D-7507, July 1974.

[30]Bradshaw, P., "Compressible Turbulent Shear Layers," *Annual Review of Fluid Mechanics*, Vol. 9, 1977, pp. 33–54.

[31]Cebeci, T., "Calculation of Compressible Turbulent Boundary Layers with Heat and Mass Transfer," *AIAA Journal*, Vol. 9, No. 6, 1971, pp. 1091–1097.

[32]Christoph, G. H., Lessmann, R. C., and White, F. M., "Calculation of Turbulent Heat Transfer and Skin Friction," *AIAA Journal*, Vol. 11, No. 7, 1973, pp. 1046–1048.

[33]Schlichting, H., *Boundary-Layer Theory*, 7th ed., McGraw–Hill, New York, 1987, pp. 633–643.

[34]Hartunian, R. A., Russo, A. L., and Marrone, P. V., "Boundary-Layer Transition and Heat Transfer in Shock Tubes," *Journal of the Aerospace Sciences*, Vol. 27, 1960, pp. 587–594.

[35]Jones, J., "Experimental Investigation of Attenuation of Strong Shock Waves in a Shock Tube with Hydrogen and Helium Driver Gases," NACA TN 4072, July 1957.

[36]Emrich, R. J., and Curtis, C. W., "Attenuation in the Shock Tube," *Journal of Applied Physics*, Vol. 24, No. 3, 1953, pp. 360–363.

[37]Glass, I. I., and Martin, W. A., "Experimental and Theoretical Aspects of Shock-Wave Attenuation," *Journal of Applied Physics*, Vol. 26, No. 1, 1955, pp. 113–120.

[38]Donaldson, C. duP., and Sullivan, R. D., "The Effect of Wall Friction on the Strength of Shock Waves in Tubes and Hydraulic Jumps in Channels," NACA TN 1942, Sept. 1949.

[39]Hollyer, R. N., "Attenuation in the Shock Tube: I. Laminar Flow," *Journal of Applied Physics*, Vol. 27, No. 3, 1956, pp. 254–261.

[40]Mirels, H., "Attenuation in a Shock Tube due to Unsteady-Boundary-Layer Action," NACA Rept. 1333, 1957; also NACA TN 3278, Aug. 1956.

[41]Rosciszewski, J., "Influence of Shock-Wave Attenuation by Boundary-Layer Growth on Contact-Surface Motion in a Shock Tube," *Journal of the Aerospace Sciences*, Vol. 26, No. 6, 1959, pp. 388, 389.

[42]de Boer, P. C. T., and Miller, J. A., "Boundary Layer Effects on Density Measurements in Shock Tubes," *Modern Developments in Shock Tube Research, Proceedings of the Tenth International Shock Tube Symposium*, edited by G. Kamimoto, Shock Tube Research Society, Kyoto, Japan, 1975, pp. 796–807.

[43]Zeitoun, D., Brun, R., and Valetta, M.-J., "Shock-Tube Flow Computation Including the Diaphragm and Boundary-Layer Effects," *Shock Tubes and Waves, Proceedings of the 12th International Symposium on Shock Tubes and Waves*, edited by A. Lifshitz and J. Rom, Magnes Press, Jerusalem, 1979, pp. 180–186.

[44]Mirels, H., and Braun, W. H., "Nonuniformities in Shock-Tube Flow due to Unsteady-Boundary-Layer Action," NACA TN 4021, May 1957.

[45]Davidson, D. F., Bates, R. W., Petersen, E. L., and Hanson, R. K., "Shock Tube Measurements of the Equation of State of Argon," *International Journal of Thermophysics*, Vol. 19, No. 6, 1998, pp. 1585–1594.

[46]Petersen, E. L., Bates, R. W., Davidson, D. F., and Hanson, R. K., "Laser Absorption and Infrared Emission Measurements in a High-Pressure Shock Tube," AIAA Paper 97-0316, Jan. 1997.

G. V. Candler
Associate Editor